PC-AGL: Light-Weighted Prior Constrained Adaptive Graph Learning for fMRI Analysis to Diagnose Autism Spectrum Disorders

1st Wenbo Ning
School of Software
Taiyuan University of Technology
Taiyuan, China
2023521874@link.tyut.edu.cn

2nd Shijie Guo
School of Software
Taiyuan University of Technology
Taiyuan, China
2023521863@link.tyut.edu.cn

3rd Yuxiang Guo
School of Software
Taiyuan University of Technology
Taiyuan, China
sxtygyx@163.com

4th Yan Niu
College of Computer Science and Technology
Taiyuan University of Technology
Taiyuan, China
niuyan@tyut.edu.cn

5th Rui Cao
School of Software
Taiyuan University of Technology
Taiyuan, China
caorui@tyut.edu.cn

6th Xin Wen*
School of Software
Taiyuan University of Technology
Taiyuan, China
xwen@tyut.edu.cn

***Abstract*—Resting-state functional magnetic resonance imaging (rs-fMRI)-derived functional connectivity (FC) has emerged as a potent metric for analyzing neuropsychiatric disorders, with autism spectrum disorder (ASD) being a prime focus. However, existing deep learning-based automated diagnostic methodologies suffer from several limitations, including the neglect of global representations, excessive parameterization, and insufficient interpretability. In this study, we propose a novel prior constrained adaptive graph learning (PC-AGL) method for ASD diagnosis. Firstly, a graph model integrated with a priori constraints is constructed on the basis of discriminative FC. Subsequently, a comprehensive convolutional kernel is devised to amalgamate short-range and long-range representations. The Autism Brain Imaging Data Exchange (ABIDE) dataset is employed for ASD detection. Our results indicate that the PC-AGL approach achieves an accuracy of 73% in ASD identification, while concurrently reducing the training parameters by 85% compared to the state-of-the-art model. The reduction in model parameters not only showcases its potential for deployment in edge computing applications but also the discriminative patterns unveiled may offer data-driven insights into the underlying brain-neurological mechanisms of ASD.**

***Index Terms*—Graph Learning, Prior Constrained, fMRI, Functional Connectivity, Autism Spectrum Disorders**

I. Introduction

Alterations in functional connectivity (FC) have been suggested as potential clinical neuroscience biomarkers to facilitate the diagnosis of neurodevelopmental disorders, such as autism spectrum disorders (ASD) [1] [2]. The majority of diagnoses of such psychiatric disorders rely on the evaluations by clinical experts and these cognitive assessments may lead to objective biases [3] [4] [5]. Recently, computer-aided diagnosis (CAD) using rs-fMRI has attracted the interest of researchers [6] [7],especially for the connectomic approaches [8].

* is the corresponding author.

The connectomic CAD integrates machine learning and deep learning methods including support vector machine, deep neural networks (DNNs) [9], convolutional neural networks (CNNs) [10], and graphic convolutional networks (GCNs) [11], with CNNs-based approaches predominating. CNNs rely on local receptive fields to learn short-range representations but lack global perspective capture [12]. In contrast, brain functional connectivity naturally fits graph structures, and GCNs can comprehensively learn brain topology—via multilayer stacking, they effectively capture local/global relationships among brain regions of interest (ROIs), facilitating analysis of inter-regional complex interactions (especially fMRI time series correlations) [13] and handling both node (brain region) static features and edge (FC) features [14]. For instance, Graph Attention Network (GAT) (GNN with attention mechanism) achieved 72.40% ASD detection accuracy [15]; higher-order node embedding and ROI location coding improved major depressive disorder detection [16]; Dynamic Graph Convolutional Network (dGCN) utilized dynamic graphs to attain 72.0% accuracy on ADHD dataset [17]. However, existing GCNs for functional connectivity lack prior knowledge guidance, and the constructed brain graphs suffer from redundant connections and low signal-to-noise ratio, often leading to suboptimal outcomes.

Consequently, methods leveraging complementary strengths of CNNs and GCNs are required. A common approach treats functional connectivity as images to learn local features via 2D convolutional kernels [18], [19], but it relies on pixel spatial neighborhoods rather than ROI positional/functional relationships, neglecting FC topological information. To address this, BrainNetCNN [20] incorporated edge-to-edge (E2E), edge-to-node (E2N), and node-to-graph (N2G) modules, enabling prediction of cognitive/motor developmental scores for preterm infants' structural networks with lower computational cost than GCNs. Its core modules also enhance CAD classifica-

tion performance [21]. Nevertheless, BrainNetCNN assumes uniform connection counts across ROIs (overlooking neural activity differences), assigns identical convolutional kernels to all brain regions (disregarding heterogeneity), and treats all FC connections as valid (increasing harmful information redundancy for model training).

Another solution employs an element-wise weighting mechanism to update node representations [22], enhancing ROI convolutional connectivity, but sequential ROI-wise convolution significantly reduces computational efficiency. Focusing on functional brain network topology, conditional Graph Convolutional Network (cGCN) [23] applied to FCs achieved 70.7% classification accuracy on ABIDE [24]. However, cGCN-based methods overlook brain region heterogeneity, either ignoring brain network topology's impact on representation learning or being constrained by assumptions (e.g., uniform ROI connection counts), which may lead to inaccurate diagnostic support.

To address the above issues, we propose a prior constrained adaptive graph learning (PC-AGL) to diagnose ASD, which effectively captures topological information by defining an adaptive convolutional neighborhoods and focusing on the heterogeneity between specific brain regions. The experimental results on ABIDE demonstrate that, under the same circumstances, PC-AGL can achieve performance close to that of the state-of-the-art methods while significantly reducing the model parameters. Meanwhile, the ablation experiments have verified the effectiveness of PC-AGL. The confusion experiments indicate that even when the label error rate reaches 30%, PC-AGL can still maintain a relatively good performance, further proving the effectiveness of the proposed method. The main contributions of this work include three aspects:

- The contrast mask has the ability to conduct statistical analysis on the functional pattern of brain activity and subsequently impose constraints on the convergence of model training.
- To fully understand the heterogeneity between brain regions, we conduct the adaptive aggregation of ROIs graph-level representations.
- The proposed method surpasses existing works in the aspect of classification. Its structure is relatively simple and fundamental, and the number of its parameters is significantly fewer than that of the GNN-based methods.

The c hapter 2 of this paper introduces the PC-AGL framework. In Chapter 3, comparative experiments are designed, and ablation and confusion experiments verify the superiority and robustness of the model. Chapter 4 discusses the key factors affecting masking performance, and disease-related biomarkers are explored through masking experiments.

II. Method

A. Proposed PC-AGL

PC-AGL comprises three components: prior mask construction, graph learning and classification, and loss optimization (Fig. 1) A statistical contrast mask was derived from functional connectivity differences between ASD and HC groups in the training set. Graph convolution operates exclusively on edges preserved in this mask, ensuring biologically relevant neighborhood constraints. Ultimately, Node features are updated via masked aggregation and classified through an MLP.

1) Construction of contrast mask: The objective of the module is to generate a comparison mask by a prior information that most accurately characterises the differences between patient and normal human brain networks. In more detail, a FC is generated by calculating the Pearson correlation (PCC) between ROI's time series in order to obtain the connectivity patterns between whole-brain ROIs. Two-sample t-tests were performed on the FC of the training set data for each cross-validation split, yielding the difference matrix P.The data acquisition process is inherently limited, which results in the acquisition of neural images from different data sites that exhibit a range of noise characteristics. In order to obtain a more precise brain link network, these noises can be efficiently eliminated through the process of thresholding. Networks constructed with lower thresholds exhibit a reduction in the number of connections, thereby facilitating a more discernible topological relationship between brain regions. In contrast, brain networks constructed with higher thresholds may exhibit a greater degree of noise. For the P matrix, the connectivity of the edges is filtered by a threshold, below which connections are considered to exist, and vice versa. To ensure optimal performance, the threshold value should range from 0.1 up to 0.0001. By mapping the binarised direct connection A as a mask onto the adjacency matrix of a graph, the most discriminative brain network connectivity relations are automatically brought to the fore.

2) Adaptive graph convolution: The fMRI image is divided into ROIs based on the selected atlas. Each ROI is considered as a node, and functional connections between any two ROIs are considered as edges. The graph is defined as $G = (V, E)$, where $V = \{v_1, ..., v_n\}$ represents the set of nodes (ROIs), and E is the set of edges, the (v_i, v_j) set of vertices connecting v_i to v_j. Following masking by the A matrix, each node is connected solely to a diminished number of other nodes. In particular, the number of neighbours associated with each brain region is not constant, but is rather defined by the number specified in the A matrix. This guarantees that brain regions which are classified as 'hubs' will have a greater number of neighbours.

In this paper, the edge convolution approach, as derived from reference Wang [25], is employed for the implementation of the graph convolution layer.

$$x_i^{'} = \max_{j:(i,j)\in\epsilon} h_\theta(x_i||x_j - x_i) \tag{1}$$

In Equation 1, x_i denotes the feature vector of the central node v_i and x_j is the feature of the neighbouring node v_j with which it is connected. In addition to the original feature of the central node, the node value difference is $x_j - x_i$ added as a supplementary feature. h_θ represents the nonlinear activation function, which is implemented by the MLP and the

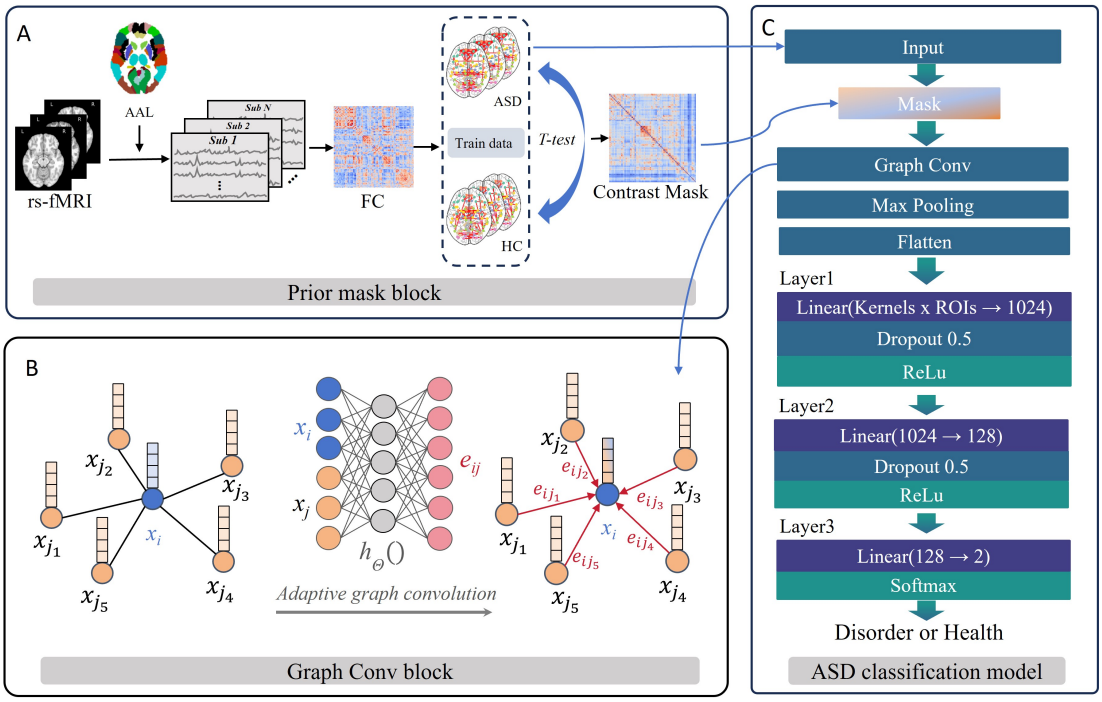

Fig. 1: The overview of our proposed PC-AGL. A) The prior mask block generates a contrastive mask by utilising the data from the training set, thereby characterising the differences between the brains of the two groups of subjects. B) The edge convolution module performs feature computation through the acquisition of structural information from the selected brain network. C) Flow of the proposed model.

corrected linear unit (ReLU) in Equation 2. Here θ denotes the trainable parameter. The characteristic convolution output $x_i^{'}$ is the maximum activation value of its neighborhood.

$$\begin{aligned} x_j^{'} &= \max_{j:(i,j)\in\epsilon} (ReLU(x_i||x_j - x_i)) \\ &= \max_{j:(i,j)\in\epsilon} (max(0, (ReLU(x_i||x_j - x_i))) \end{aligned} \tag{2}$$

In consideration of the considerable heterogeneity between brain regions, the input FCs is subjected to processing through a contrast mask containing a priori information, thereby facilitating the acquisition of a differentiated representation that is pertinent to group discriminatory information. This is due to the fact that the contrast mask captures the relevance of connectivity relationships between brain regions in relation to disease classification, while also mitigating the issue of overfitting. The masking process can be described in Equation 3:

$$x_i = a_i \cdot FC_i \tag{3}$$

where the $a_i \in \mathbb{R}^{1xN}$ represents line i of the A matrix, $FC_i \in \mathbb{R}^{1xN}$ represents line i of the function connection. For reasons of save computing resources and Memory, in the concrete implementation, this article will x_i compressed into $a_i \in \mathbb{R}^{1x\,max(k)}$, k is the length of the node representation vector.

3) Loss function: In this work, we use the binary cross entropy as the loss function and the Adam optimizer for model training, which can be described by Equation 4.

$$\begin{aligned} L_{BCE} &= \frac{1}{N}\sum_i L_i \\ &= \frac{1}{N}\sum_i -[y_i \cdot \log(p_i) + (1-y_i)\log(1-p_i)] \end{aligned} \tag{4}$$

where y_i represents the label of the sample i, and p_i represents the probability that the sample i is predicted to be positive class. In order to prevent the classifier from overfitting, we incorporate $L2$ loss into the classifier layer., as shown in Equation 5:

$$L_{classifer} = \lambda \sum_{i=1}^{n} w_i^2 \tag{5}$$

where, w_i is the parameter of the classifier layer. The total loss function is shown in shown in Equation 6:

$$L = L_{BCE} + L_{classifer} \tag{6}$$

III. Experiments and Results

A. Dataset and Preprocessing

The Autism Brain Imaging Data Exchange I (ABIDE) dataset, a publicly available multi-site resource, provided phenotypic and imaging data for 1,112 participants (539 ASD, 573

TABLE I: THE RESULTS OF THE COMPARISON EXPERIMENTS UNDER TEN-FOLD CROSS VALIDATION.

Method	Accuracy (%)	Sensitivity (%)	Specificity (%)	AUC (%)	Params (M)	FLOPs (MFlops)
Logistic Regression	64.4 ± 1.4	61.5 ± 3.1	66.3 ± 1.3	68.0 ± 2.1	-	-
SVM(linear kernel)	62.4 ± 1.2	59.6 ± 1.9	64.2 ± 3.5	65.6 ± 2.2	-	-
BrainNetCNN [20]	66.5 ± 1.4	62.6 ± 0.7	69.7 ± 2.0	71.2 ± 1.3	-	-
BrainTGL [26]	67.8 ± 1.7	62.2 ± 1.9	72.9 ± 1.8	67.6 ± 1.5	-	-
LCC-FC [27]	67.9 ± 0.9	65.5 ± 3.9	70.4 ± 3.3	71.5 ± 1.0	-	-
BrainNetCNN [20]	66.5 ± 1.4	62.6 ± 0.7	69.7 ± 2.0	71.2 ± 1.3	0.6	56.9
ASD-DiagNet [28]	68.1 ± 1.0	60.0 ± 1.0	75.0 ± 1.4	67.5 ± 1.0	5.6	**11.1**
BolT [29]	71.3 ± 4.6	64.8 ± 7.9	–	**77.6 ± 3.4**	-	-
cGCN [23]	71.6 ± 0.7	65.2 ± 1.5	73.0 ± 1.3	73.2 ± 1.2	2.0	102.6
Our method(PC)	72.7 ± 0.5	68.7 ± 1.0	76.0 ± 0.8	74.8 ± 0.9	**0.3**	32.8
Our method	**73.0 ± 0.8**	**67.2 ± 2.6**	**78.0 ± 1.2**	74.8 ± 0.9	15.3	46.9

Note: PC Indicates parameter compression, All models are experimented on AAL116 atlas.

typically developing controls; ages 6–64). Following HIPAA-compliant anonymization per INDI protocols, 884 subjects (408 ASD, 476 controls; ages 7–64) were included after quality screening. fMRI data underwent C-PAC preprocessing (0.01–0.1 Hz bandpass filtering, no global signal regression) [30]. Four brain atlases (AAL116 [31], CC200 [32], CC400 [33], Harvard Oxford [34]) defined 116, 200, 400, and 90 regions of interest. ROI time series were z-score normalized across subjects for model input.

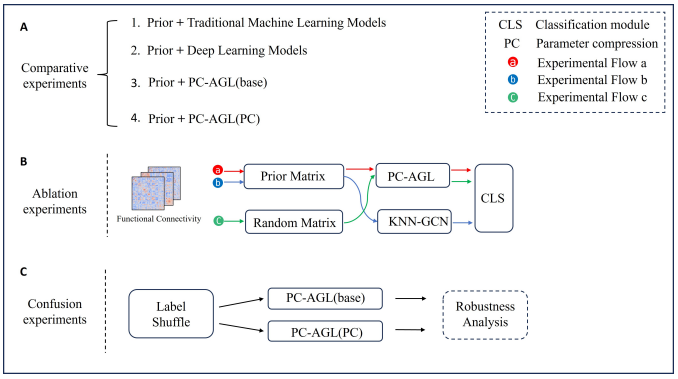

Fig. 2: Experimental Setting. A) The comparison experiments are divided into four parts. Under the premise of the same prior, PC-AGL(base) was compared with machine learning methods, deep learning methods, and the model compressed PC-AGL(PC). B) The ablation experiments aim to demonstrate the importance of the prior information and the adaptive graph convolution module respectively. A total of three groups are set up, which are: prior+PC-AGL, prior+KNN-GCN, and random mask+PC-AGL. C) The confusion experiments were conducted to assess model robustness by progressively shuffling the labels in the training set to varying degrees and subsequently evaluating model performance on the unaltered test set.

B. Experimental Settings

The performance of PC-AGL was rigorously evaluated through comparison experiments, ablation experiments, and confusion study, as illustrated in Fig. 2. Furthermore, we conducted ROI occlusion experiments to identify potential biomarkers that may facilitate disease classification or advance our mechanistic understanding of disease pathogenesis. All reported results represent the mean values obtained from ten-fold cross validation to mitigate stochastic variability.

C. Parameter Settings

All experiments were implemented in PyTorch. A prior mask was thresholded at $p = 0.05$. Optimization used Adam with adaptive learning rate, lower-bounded at 10^{-6}. Model weights were saved only upon validation accuracy improvement. L_2 regularization was applied, with optimal coefficients selected from $0.1, 0.01, 0.001, 0.0001$. For fair comparison in comparison and ablation experiments, batch size was fixed at 10; other hyperparameters followed original model defaults [20], [22], [23], [25]. In cGCN, the final RNN layer was removed since input functional connectivity matrices lack temporal structure. SVM and logistic regression used 1000 iterations and default hyperparameters.

D. Quantification and statistical analysis

Model performance was evaluated using accuracy, sensitivity, specificity, and area under the curve (AUC).

$$Accuracy(ACC) = \frac{TP + TN}{TP + TN + FP + FN} \tag{7}$$

$$Sensitivity(SEN) = \frac{TP}{TP + FN} \tag{8}$$

$$Specificity(SPE) = \frac{TN}{TN + FP} \tag{9}$$

$$Area\ under\ the\ curve(AUC) = \frac{1}{2} \sum_{i=1}^{m-1} (x_{i+1} - x_i)(y_{i+1} - y_i) \tag{10}$$

TP, TN, FP, and FN denote true positive, true negative, false positive, and false negative counts. AUC is computed via trapezoidal integration of the ROC curve, where x_i and y_i represent false positive rate and true positive rate at each point.

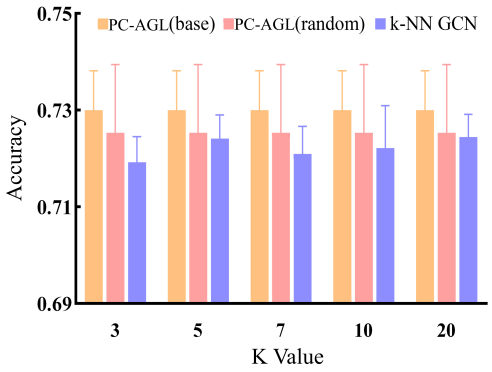

Fig. 3: Ablation experiments.

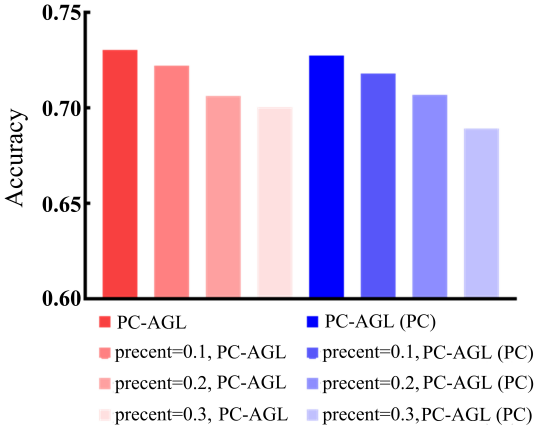

Fig. 4: Confusion experiments.

E. Experimental Results

1) Comparison Experiments: The comparison experiments entailed the utilisation of identical prior information in determining the convolutional neighbourhood by all methods. As shown in Table 1, the proposed adaptive graph convolution model method captures the differences in brain networks using prior information and exhibits superior performance. The accuracy of this model is 73.0%, the sensitivity is 67.2%, the specificity is 78.0%, and the AUC is 74.8%, which is significantly better than existing methods.

PC-AGL also employs a parameter compression technique, significantly reducing the number of parameters with minimal performance degradation. The original PC-AGL has 15.3M parameters, the highest among lightweight networks. To further reduce parameters, we replaced fully-connected layers with convolutional layers, resulting in the parameter compressed version, PC-AGL(PC), which has 0.3M parameters and 32.8M FLOPs. This version outperforms BrainNetCNN, ASD-DiagNet, and cGCN in accuracy while requiring fewer computations. Shallow deep learning architectures typically reduce parameters through matrix multiplication, but the large dimension of functional connectivity (6670 after flattening the AAL atlas) increases parameter count when fully-connected layers are used. Replacing them with convolutional layers reduces parameters but can impair performance [35]. PC-AGL(PC) mitigates this issue through prior constraints, balancing model size and performance. This lightweight architecture facilitates rapid deployment and fine-tuning for fMRI-based disease diagnosis, demonstrating PC-AGL's efficient model design with low parameter redundancy.

2) Ablation Experiments: To validate the effectiveness of each module in the proposed PC-AGL, an experimental study was conducted on each individual module (Fig. 3). Specifically, the prior information was replaced with randomly generated matrices to construct PC-AGL(random), which was then compared with PC-AGL(base) that used the prior information. This was done to verify the effectiveness of the prior information guidance. Furthermore, the adaptive graph convolution module was substituted by a module that applied the k-Nearest Neighbors (k-NN) algorithm to determine the convolutional neighborhood of cGCN (where k represents the number of neighbors considered for each ROI) [25], [36], to ascertain the efficacy of adaptive graph convolution in aggregating neighbourhood information. In the ablation experiment scenario, the k-NN+GCN model reaches its optimal performance when k = 5. However, this performance is still considerably lower than that of PC-AGL(base), suggesting that the adaptive graph convolution module can understand the heterogeneity of brain regions and has the ability to extract discriminatory features (Fig. 3). Notably, compared with PC-AGL(random), PC-AGL(base) shows higher efficiency, stability, and portability.

3) Confusion Study: To assess robustness to label noise, we conducted confusion experiments using AAL atlas based FC, the atlas that yielded the highest accuracy in prior comparison and ablation experiments. Training labels were randomly disrupted at 10%, 20%, and 30% , and validation accuracy was used as the primary evaluation metric. PC-AGL achieved 73.7% accuracy with clean labels, declined by only 0.8% to 72.9% at 10% disrupted labels, and remained above 70% at 30% disrupted labels. PC-AGL(PC) and PC-AGL(base) showed similar degradation patterns, indicating that parameter compression preserves discriminative capacity under label corruption and that the full model is robust to label errors (Fig. 4).

TABLE II: THE TOP TEN BRAIN REGIONS WITH THE HIGHEST CLASSIFICATION CONTRIBUTIONS IN THE AAL ATLAS.

Index	Brain Regions	Degradation (%)
8	Middle frontal gyrus (R)	2.147
55	Fusiform gyrus (L)	1.243
38	DaHippocampus (R)	0.960
31	Anterior cingulate gyrus (L)	0.847
100	Cerebellum 6 (R)	0.791
96	Cerebellum 3 (R)	0.791
88	Temporal pole (middle) (R)	0.734
46	Cuneus (R)	0.734
35	Posterior cingulate gyrus (L)	0.678
14	Inferior frontal gyrus (triangular) (R)	0.678

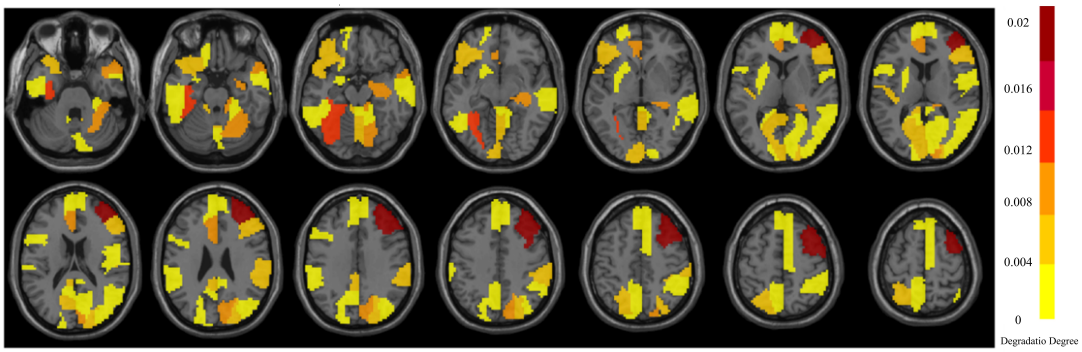

Fig. 5: Activation patterns of brain regions obtained by PC-AGL. The utilisation of darker colour representations of brain regions exerted a more substantial influence on model performance, thereby indicating that these regions may assume a pivotal role in disease discrimination.

4) Occlusion experiments: The masking method [37] was used to identify key ROIs for classification by training the model to zero out individual regions and evaluating performance degradation. The resulting blocking pattern was mapped to the cortical surface (Fig. 5). The occlusion experiment divided the dataset into training, validation, and testing sets with a ratio of 2.67:1.33:1, and was repeated 10 times to eliminate random influences. The ten most significant brain regions for classification were identified, as shown in Table II, including the right middle frontal gyrus, left fusiform gyrus, right hippocampus, among others, exhibit pronounced lateralization.

Prior studies have linked these regions to ASD, such as the fusiform gyrus and frontal cortex showing structural asymmetries [38], and hippocampus involvement [39]. Functional connectivity changes in the cingulate cortex and temporal gyrus are also potential biomarkers for ASD behaviors [40]. Our findings align with these results.

Additionally, while GCNs typically aggregate local ROI features, fMRI based CAD studies face limitations in local receptive fields and incomplete information aggregation. By enhancing the GCN to incorporate both local and global brain connectivity information through selective aggregation, we improved classification performance while maintaining a lightweight model. The occlusion and confusion experiments validate the robustness and efficacy of this approach, offering a new direction for lightweight CAD.

IV. Discussion

Sparse representation enhances classification performance and reduces model parameters, enabling lightweight models. However, studies show that applying a two-sample T-test or specifying sparsity introduces additional hyperparameters, with no fixed optimal value established [41]. The optimal parameter is typically determined by the model's overall robustness, though sparse representation may vary across folds in cross validation. In previous research, the final sparse representation is often derived from repeated experiments or meta-analysis [41]. Factors like equipment differences, data volume, and noise can affect statistical results, leading to instability [42]. Therefore, in this paper, the prior construction adopts the overlapping part of multiple two-sample t-tests between individuals with ASD and HC in the training set. Different P-values lead to variations in the performance of PC-AGL. Hyperparameter optimization is carried out within the range of p, spanning from 0.1 to 0.0001 and within the HO110, AAL116, CC200, CC400 atlas (Fig. 6). Among these, PC-AGL attains its optimal performance when p equals 0.05 with AAL atlas, achieving an average accuracy of 73.0%. Moreover, the classification performance of the model deteriorates as the restriction on the p becomes increasingly stringent. When p is set to 0.001, the average accuracy of PC-AGL remains approximately 70%, suggesting that our model can depend on a limited number of precise features to acquire a robust and stable feature representation. Meanwhile, even if the p is loosened to 0.1, although the classification performance is still considerably lower compared to the optimal settings, the computational consumption is significantly increased. The p

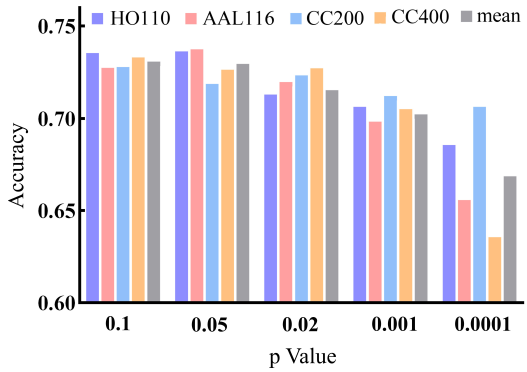

Fig. 6: Hyperparameter optimization. The overall performance of the model generally shows a decreasing trend as the P-value gradually decreases.

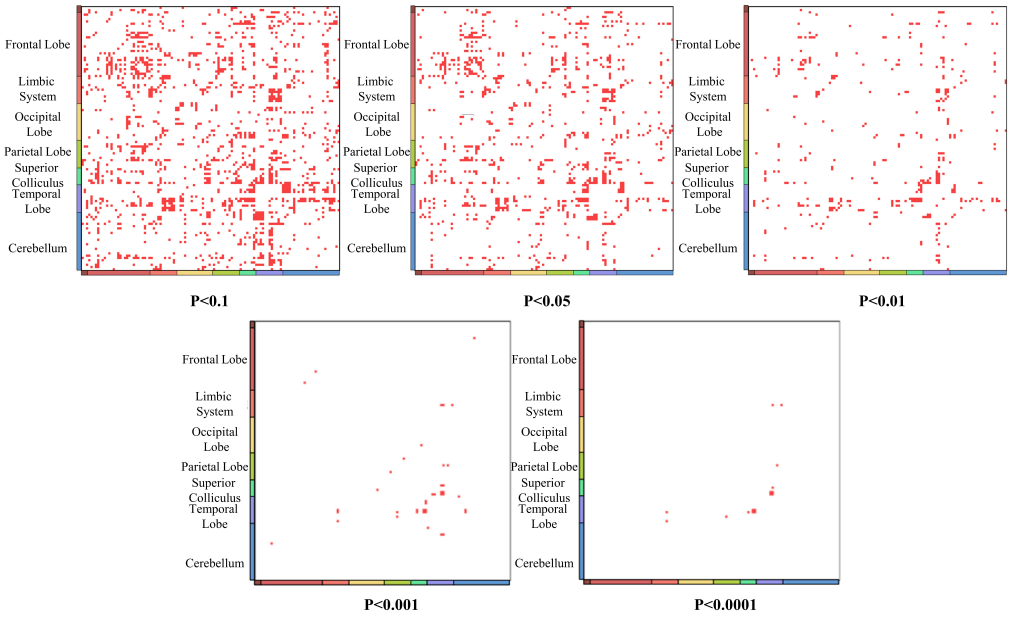

Fig. 7: Visualization of prior information. In the AAL atlas, as the p-value constraint was progressively strengthened, fewer critical brain regions were retained in the mask, while the model demonstrated optimal performance at $p < 0.05$.

of 0.05 serves not only as a statistically significant threshold but also proves to be the best in terms of both classification performance and computational consumption.

As p becomes stricter, prior information emphasizes regions like the temporal lobe, superior colliculus, parietal lobe, and limbic system, which overlap with brain regions identified in the masking experiments (Fig. 7). These regions are strongly linked to ASD [41]. With $p = 0.05$, repeated experiments yield an optimal model, balancing classification performance and parameter count. In these experiments, the AAL atlas shows significant loss reduction after 15 epochs, with convergence after 50 epochs.

V. Conclusions

In this study, the graph convolution method of prior information obtained by PC-AGL model through statistical test can effectively distinguish ASD patients from HC population. The proposed a priori is effective for various graph segmentation data, providing novel insights for future related studies. The graph convolutional module adaptively convolves different brain regions, making it suitable for the highly heterogeneous data in the brain. Furthermore, due to its shallow model structure, the PC-AGL model is easy to tune, highly efficient, and deployable on mobile devices, with a wide range of potential applications. However, PC-AGL does have some limitations. To utilize the graphic convlutional module, a front mask layer is required, which limits high parallel efficiency in some high-speed computation scenarios. In this study, we plan to experiment with several ways to construct the prior information further, aiming to find a better approach.In subsequent work We will also extend PC-AGL to different brain disease to verify its adaptability across a wide domain.

VI. Acknowledgment

This work was supported by the National Natural Science Foundation of China (62206196).

References

[1] E. Bullmore and O. Sporns, "Complex brain networks: graph theoretical analysis of structural and functional systems," *Nature reviews neuroscience*, vol. 10, no. 3, pp. 186–198, 2009.

[2] M. D. Greicius, K. Supekar, V. Menon, and R. F. Dougherty, "Resting-state functional connectivity reflects structural connectivity in the default mode network," *Cerebral cortex*, vol. 19, no. 1, pp. 72–78, 2009.

[3] H.-Y. Zhang, S.-J. Wang, J. Xing, B. Liu, Z.-L. Ma, M. Yang, Z.-J. Zhang, and G.-J. Teng, "Detection of pcc functional connectivity characteristics in resting-state fmri in mild alzheimer's disease," *Behavioural brain research*, vol. 197, no. 1, pp. 103–108, 2009.

[4] M. R. Brier, J. B. Thomas, A. M. Fagan, J. Hassenstab, D. M. Holtzman, T. L. Benzinger, J. C. Morris, and B. M. Ances, "Functional connectivity and graph theory in preclinical alzheimer's disease," *Neurobiology of aging*, vol. 35, no. 4, pp. 757–768, 2014.

[5] C. Ecker, S. Y. Bookheimer, and D. G. Murphy, "Neuroimaging in autism spectrum disorder: brain structure and function across the lifespan," *The Lancet Neurology*, vol. 14, no. 11, pp. 1121–1134, 2015.

[6] P. Raghavaiah and S. Varadarajan, "A cad system design to diagnosize alzheimers disease from mri brain images using optimal deep neural network," *Multimedia Tools and Applications*, vol. 80, no. 17, pp. 26 411–26 428, 2021.

[7] R. Qin, T. Li, C. Li, L. Li, X. Wang, and L. Wang, "Investigating altered brain functional hubs and causal connectivity in coronary artery disease with cognitive impairment," *PeerJ*, vol. 11, 2023.

[8] T. P. Johnson and A. Nath, "Biotypes of hiv-associated neurocognitive disorders based on viral and immune pathogenesis," *Current opinion in infectious diseases*, vol. 35, no. 3, pp. 223–230, 2022.

[9] H. Jang, S. M. Plis, V. D. Calhoun, and J.-H. Lee, "Task-specific feature extraction and classification of fmri volumes using a deep neural network initialized with a deep belief network: Evaluation using sensorimotor tasks," *NeuroImage*, vol. 145, pp. 314–328, 2017.

[10] M. N. I. Qureshi, J. Oh, and B. Lee, "3d-cnn based discrimination of schizophrenia using resting-state fmri," *Artificial intelligence in medicine*, vol. 98, pp. 10–17, 2019.

[11] E. N. Pitsik, V. A. Maximenko, S. A. Kurkin, A. P. Sergeev, D. Stoyanov, R. Paunova, S. Kandilarova, D. Simeonova, and A. E. Hramov, "The topology of fmri-based networks defines the performance of a graph neural network for the classification of patients with major depressive disorder," *Chaos, Solitons & Fractals*, vol. 167, p. 113041, 2023.

[12] L. Liu, F.-X. Wu, Y.-P. Wang, and J. Wang, "Multi-receptive-field cnn for semantic segmentation of medical images," *IEEE Journal of Biomedical and Health Informatics*, vol. 24, no. 11, pp. 3215–3225, 2020.

[13] R. Liu, Z.-A. Huang, Y. Hu, L. Huang, K.-C. Wong, and K. C. Tan, "Spatio-temporal hybrid attentive graph network for diagnosis of mental disorders on fmri time-series data," *IEEE TRANSACTIONS ON EMERGING TOPICS IN COMPUTATIONAL INTELLIGENCE*, 2024 APR 17 2024.

[14] Y. Yang, C. Ye, and T. Ma, "A deep connectome learning network using graph convolution for connectome-disease association study," *NEURAL NETWORKS*, vol. 164, pp. 91–104, JUL 2023.

[15] C. Yang, P. Wang, J. Tan, Q. Liu, and X. Li, "Autism spectrum disorder diagnosis using graph attention network based on spatial-constrained sparse functional brain networks," *Computers in Biology and Medicine*, vol. 139, p. 104963, 2021. [Online]. Available: https://www.sciencedirect.com/science/article/pii/S0010482521007575

[16] S. Liu and R. Gui, "Fusing multi-scale fmri features using a brain-inspired multi-channel graph neural network for major depressive disorder diagnosis," *Biomedical Signal Processing and Control*, vol. 90, p. 105837, 2024. [Online]. Available: https://www.sciencedirect.com/science/article/pii/S1746809423012703

[17] K. Zhao, B. Duka, H. Xie, D. J. Oathes, V. Calhoun, and Y. Zhang, "A dynamic graph convolutional neural network framework reveals new insights into connectome dysfunctions in adhd," *NeuroImage*, vol. 246, p. 118774, 2022. [Online]. Available: https://www.sciencedirect.com/science/article/pii/S1053811921010466

[18] Z. Sherkatghanad, M. Akhondzadeh, S. Salari, M. Zomorodi-Moghadam, M. Abdar, U. R. Acharya, R. Khosrowabadi, and V. Solari, "Automated detection of autism spectrum disorder using a convolutional neural network," *FRONTIERS IN NEUROSCIENCE*, vol. 13, JAN 14 2020.

[19] M. J. Leming, S. Baron-Cohen, and J. Suckling, "Single-participant structural similarity matrices lead to greater accuracy in classification of participants than function in autism in mri," *MOLECULAR AUTISM*, vol. 12, no. 1, MAY 10 2021.

[20] J. Kawahara, C. J. Brown, S. P. Miller, B. G. Booth, V. Chau, R. E. Grunau, J. G. Zwicker, and G. Hamarneh, "Brainnetcnn: Convolutional neural networks for brain networks; towards predicting neurodevelopment," *NeuroImage*, vol. 146, pp. 1038–1049, 2017.

[21] J. Huang, M. Wang, H. Ju, Z. Shi, W. Ding, and D. Zhang, "Sd-cnn: A static-dynamic convolutional neural network for functional brain networks," *Medical Image Analysis*, vol. 83, p. 102679, 2023. [Online]. Available: https://www.sciencedirect.com/science/article/pii/S1361841522003073

[22] J. Ji, X. Xing, Y. Yao, J. Li, and X. Zhang, "Convolutional kernels with an element-wise weighting mechanism for identifying abnormal brain connectivity patterns," *PATTERN RECOGNITION*, vol. 109, JAN 2021.

[23] L. Wang, K. Li, and X. P. Hu, "Graph convolutional network for fmri analysis based on connectivity neighborhood," *NETWORK NEUROSCIENCE*, vol. 5, no. 1, pp. 83–95, FEB 2021.

[24] A. Di Martino, C.-G. Yan, Q. Li, E. Denio, F. X. Castellanos, K. Alaerts, J. S. Anderson, M. Assaf, S. Y. Bookheimer, M. Dapretto *et al.*, "The autism brain imaging data exchange: towards a large-scale evaluation of the intrinsic brain architecture in autism," *Molecular psychiatry*, vol. 19, no. 6, pp. 659–667, 2014.

[25] Y. Wang, Y. Sun, Z. Liu, S. E. Sarma, M. M. Bronstein, and J. M. Solomon, "Dynamic graph cnn for learning on point clouds," *ACM TRANSACTIONS ON GRAPHICS*, vol. 38, no. 5, NOV 2019.

[26] L. Liu, G. Wen, P. Cao, T. Hong, J. Yang, X. Zhang, and O. R. Zaiane, "Braintgl: A dynamic graph representation learning model for brain network analysis," *Computers in Biology and Medicine*, vol. 153, p. 106521, 2023.

[27] E. Kang, D.-W. Heo, J. Lee, and H.-I. Suk, "A learnable counter-condition analysis framework for functional connectivity-based neurological disorder diagnosis," *IEEE Transactions on Medical Imaging*, vol. 43, no. 4, pp. 1377–1387, 2023.

[28] T. Eslami, V. Mirjalili, A. Fong, A. R. Laird, and F. Saeed, "Asd-diagnet: A hybrid learning approach for detection of autism spectrum disorder using fmri data," *FRONTIERS IN NEUROINFORMATICS*, vol. 13, NOV 27 2019.

[29] H. A. Bedel, I. Sivgin, O. Dalmaz, S. U. Dar, and T. Çukur, "Bolt: Fused window transformers for fmri time series analysis," *Medical image analysis*, vol. 88, p. 102841, 2023.

[30] C. Craddock, S. Sikka, B. Cheung, R. Khanuja, S. S. Ghosh, C. Yan, Q. Li, D. Lurie, J. Vogelstein, R. Burns *et al.*, "Towards automated analysis of connectomes: The configurable pipeline for the analysis of connectomes (c-pac)," *Front Neuroinform*, vol. 42, no. 10.3389, 2013.

[31] N. Tzourio-Mazoyer, B. Landeau, D. Papathanassiou, F. Crivello, O. Etard, N. Delcroix, B. Mazoyer, and M. Joliot, "Automated anatomical labeling of activations in spm using a macroscopic anatomical parcellation of the mni mri single-subject brain," *NeuroImage*, vol. 15, no. 1, pp. 273–289, 2002. [Online]. Available: https://www.sciencedirect.com/science/article/pii/S1053811901909784

[32] R. C. Craddock, G. A. James, P. E. Holtzheimer, III, X. P. Hu, and H. S. Mayberg, "A whole brain fmri atlas generated via spatially constrained spectral clustering," *HUMAN BRAIN MAPPING*, vol. 33, no. 8, pp. 1914–1928, AUG 2012.

[33] A. Schaefer, R. Kong, E. M. Gordon, T. O. Laumann, X.-N. Zuo, A. J. Holmes, S. B. Eickhoff, and B. T. T. Yeo, "Local-global parcellation of the human cerebral cortex from intrinsic functional connectivity mri," *Cerebral Cortex*, vol. 28, no. 9, pp. 3095–3114, 07 2017. [Online]. Available: https://doi.org/10.1093/cercor/bhx179

[34] R. S. Desikan, F. Ségonne, B. Fischl, B. T. Quinn, B. C. Dickerson, D. Blacker, R. L. Buckner, A. M. Dale, R. P. Maguire, B. T. Hyman, M. S. Albert, and R. J. Killiany, "An automated labeling system for subdividing the human cerebral cortex on mri scans into gyral based regions of interest," *NeuroImage*, vol. 31, no. 3, pp. 968–980, 2006. [Online]. Available: https://www.sciencedirect.com/science/article/pii/S1053811906000437

[35] H.-P. Chan, R. K. Samala, L. M. Hadjiiski, and C. Zhou, "Deep learning in medical image analysis," *Deep learning in medical image analysis: challenges and applications*, pp. 3–21, 2020.

[36] K. Qin, D. Lei, W. H. Pinaya, N. Pan, W. Li, Z. Zhu, J. A. Sweeney, A. Mechelli, and Q. Gong, "Using graph convolutional network to characterize individuals with major depressive disorder across multiple imaging sites," *eBioMedicine*, vol. 78, p. 103977, 2022. [Online]. Available: https://www.sciencedirect.com/science/article/pii/S235239642200161X

[37] M. D. Zeiler and R. Fergus, "Visualizing and understanding convolutional networks," in *Computer Vision – ECCV 2014*, D. Fleet, T. Pajdla, B. Schiele, and T. Tuytelaars, Eds. Cham: Springer International Publishing, 2014, pp. 818–833.

[38] Z. Sha, D. van Rooij, E. Anagnostou, C. Arango, G. Auzias, M. Behrmann, B. Bernhardt, S. Bolte, G. F. Busatto, S. Calderoni, R. Calvo, E. Daly, C. Deruelle, M. Duan, F. L. S. Duran, S. Durston, C. Ecker, S. Ehrlich, D. Fair, J. Fedor, J. Fitzgerald, D. L. Floris, B. Franke, C. M. Freitag, L. Gallagher, D. C. Glahn, S. Haar, L. Hoekstra, N. Jahanshad, M. Jalbrzikowski, J. Janssen, J. A. King, L. Lazaro, B. Luna, J. McGrath, S. E. Medland, F. Muratori, D. G. M. Murphy, J. Neufeld, K. O'Hearn, B. Oranje, M. Parellada, J. C. Pariente, M. C. Postema, K. L. Remnelius, A. Retico, P. G. P. Rosa, K. Rubia, D. Shook, K. Tammimies, M. J. Taylor, M. Tosetti, G. L. Wallace, F. Zhou, P. M. Thompson, S. E. Fisher, J. K. Buitelaar, and C. Francks, "Subtly altered topological asymmetry of brain structural covariance networks in autism spectrum disorder across 43 datasets from the enigma consortium," *MOLECULAR PSYCHIATRY*, vol. 27, no. 4, pp. 2114–2125, APR 2022.

[39] S. M. Banker, X. Gu, D. Schiller, and J. H. Foss-Feig, "Hippocampal contributions to social and cognitive deficits in autism spectrum disorder," *Trends in Neurosciences*, vol. 44, no. 10, pp. 793–807, 2021. [Online]. Available: https://www.sciencedirect.com/science/article/pii/S0166223621001648

[40] M. Kornisch, C. Gonzalez, and T. Ikuta, "Functional connectivity of the posterior cingulate cortex in autism spectrum disorder," *PSYCHIATRY RESEARCH-NEUROIMAGING*, vol. 342, AUG 2024.

[41] S. J. C. Schielen, J. Pilmeyer, A. P. Aldenkamp, and S. Zinger, "The diagnosis of asd with mri: a systematic review and meta-analysis," *TRANSLATIONAL PSYCHIATRY*, vol. 14, no. 1, AUG 2 2024.

[42] S. M. Smith and T. E. Nichols, "Statistical challenges in "big data" human neuroimaging," *NEURON*, vol. 97, no. 2, pp. 263–268, JAN 17 2018.